Bioactive Materials 34 (2024) 401–413

Contents lists available at ScienceDirect

Bioactive Materials

journal homepage: www.keaipublishing.com/en/journals/bioactive-materials

Hydrophobic surface induced pro-metastatic cancer cells for *in vitro* extravasation models

Minseok Lee [a,1], Seunggyu Kim [b,1], Sun Young Lee [c], Jin Gyeong Son [c], Joonha Park [b], Seonghyeon Park [a], Jemin Yeun [a], Tae Geol Lee [c,**], Sung Gap Im [a,d,***], Jessie S. Jeon [b,*]

[a] Department of Chemical and Biomolecular Engineering, Korea Advanced Institute of Science and Technology, Daehak-ro 291, Yuseong-gu, Daejeon, 34141, Republic of Korea
[b] Department of Mechanical Engineering, Korea Advanced Institute of Science and Technology, Daehak-ro 291, Yuseong-gu, Daejeon, 34141, Republic of Korea
[c] Bioimaging Team, Safety Measurement Institute, Korea Research Institute of Standards and Science (KRISS), Gajeong-ro 267, Yuseong-gu, Daejeon, 34113, Republic of Korea
[d] KAIST Institute for the NanoCentury (KINC), Korea Advanced Institute of Science and Technology, Daehak-ro 291, Yuseong-gu, Daejeon, 34141, Republic of Korea

ARTICLE INFO

Keywords:
Initiated chemical vapor deposition
Cancer spheroid
Cancer extravasation
Organ-on-a-chip
In vitro disease model

ABSTRACT

In vitro vascularized cancer models utilizing microfluidics have emerged as a promising tool for mechanism study and drug screening. However, the lack of consideration and preparation methods for cancer cellular sources that are capable of adequately replicating the metastatic features of circulating tumor cells contributed to low relevancy with *in vivo* experimental results. Here, we show that the properties of cancer cellular sources have a considerable impact on the validity of the *in vitro* metastasis model. Notably, with a hydrophobic surface, we can create highly metastatic spheroids equipped with aggressive invasion, endothelium adhesion capabilities, and activated metabolic features. Combining these metastatic spheroids with the well-constructed microfluidic-based extravasation model, we validate that these metastatic spheroids exhibited a distinct extravasation response to epidermal growth factor (EGF) and normal human lung fibroblasts compared to the 2D cultured cancer cells, which is consistent with the previously reported results of *in vivo* experiments. Furthermore, the applicability of the developed model as a therapeutic screening platform for cancer extravasation is validated through profiling and inhibition of cytokines. We believe this model incorporating hydrophobic surface-cultured 3D cancer cells provides reliable experimental data in a clear and concise manner, bridging the gap between the conventional *in vitro* models and *in vivo* experiments.

1. Introduction

Metastasis, the spread of cancer cells from primary site to another organ, is estimated to be a leading cause of cancer-related death due to a poor patient prognosis [1,2]. Hence, one of the most effective methods to raise the cure rate of cancer patients is early diagnosis and prevention of metastasis. The metastatic cascade refers to the complex multistep process; separation of aggressive cancer cells from the primary tumor by losing their cell-cell junctions, invasion to stromal and endothelial barrier into the bloodstream, termed as intravasation, circulation inside of bloodstream, breaking and crossing the endothelial barrier into the metastatic sites, termed as extravasation, and finally, metastatic colonization for the formation of new tumors [3,4]. Epithelial-to-mesenchymal transition (EMT) is closely associated to the intrinsic characteristics of cancer cells during metastasis progression [5]. Cancer cells undergo EMT, lose the epithelial characteristics and acquire mesenchymal and invasive properties to shed from the primary tumor and intravasate into the peripheral blood circulating system as

Peer review under responsibility of KeAi Communications Co., Ltd.
* Corresponding author. Department of Mechanical Engineering, Korea Advanced Institute of Science and Technology, Daehak-ro 291, Yuseong-gu, Daejeon, 34141, Republic of Korea.
** Corresponding author.
*** Corresponding author.
E-mail addresses: tglee@kriss.re.kr (T.G. Lee), sgim@kaist.ac.kr (S.G. Im), jsjeon@kaist.ac.kr (J.S. Jeon).
[1] These authors contributed equally.

https://doi.org/10.1016/j.bioactmat.2023.12.021
Received 17 July 2023; Received in revised form 8 December 2023; Accepted 23 December 2023

circulating tumor class (CTCs) in the form of single cells or clusters [6]. The seed and soil mechanism has been a central hypothesis in the mechanism of metastasis, which states that both intrinsic characteristics of cancer cells, referred to as the "seed", and the local microenvironment, referred to as the "soil", are essential for the metastatic event [7]. Therefore, extravasation, which is highly related to the crosstalk between CTCs and microenvironments at metastatic sites, is suggested to be a key step in the metastatic cascade [8]. Accordingly, unveiling the nature of extravasation is of key importance for mechanism study, diagnosis, and drug screening [9].

Since metastasis consists of multisteps, detailed mechanism analysis for each step must be accompanied to suggest strategies for developing anti-metastasis therapeutics. Indeed, both *in vivo* animal experiments and various *in vitro* assays for modeling metastasis have been used for these mechanism studies. However, the limitation of *in vivo* experiments lies in the fact that detailed analysis with real-time observations of cellular events occurring during the metastasis process is practically impossible, only focusing on the input, transplantation of cancer cells, and the output, resulting in metastatic progress [10]. Moreover, conventional *in vitro* methods such as transwell migration assay make it difficult to mimic stimulation induced from surrounding cells, and physiological cell-cell and cell-ECM interface, not sufficiently replicating the *in vivo* microenvironments [11]. As a result, numerous research efforts on modeling cancer metastasis in microfluidic-based organs-on-chips have been directed toward creating a set of reliable biomedically relevant information [12]. Microfluidic chip model can provide highly controllable microenvironments where various parameters, such as types of surrounding cell interfaces, cytokines and inhibitors, can be modified [13]. Real-time imaging also enables extensive analysis of each stage of metastasis. Therefore, the microfluidic-based metastasis chip is widely regarded as a promising *in vitro* model platform that can offer detailed insights into the process of metastasis diagnosis and drug development.

Recent microfluidic research on cancer extravasation has primarily focused on replicating the pre-metastatic niche within the system, which mimics the *in vivo* microenvironment counterpart. These studies have emphasized the dynamic behaviors in the intricate process and revealed their underlying mechanisms [14–16], including tissue-specific tumor extravasation [17–19], physical factors or adhesion molecules involved in transendothelial migration [20,21], immune cell functions in cancer extravasation [22,23], and therapeutic inhibition of cancer cell migration [24]. These approaches are crucial since the fate of cancer cells is determined by the surrounding cells through direct interactions or their cytokines secretion in the tumor microenvironment [25–27]. In addition to constructing pre-metastatic microenvironments, it is also critically essential to consider which cellular source for cancer cells to utilize in the model. Particularly, EMT-undergone and circulating cells already possess metastatic features while experiencing several cellular events, including local invasion, circulation in the bloodstream, and intravasation [1]. However, many studies have relied solely on 2D cultured cancer cells that can contribute to missing meaningful results, which may not be an ideal cellular source for *in vitro* models. Unlike *in vivo* tumors, 2D cultured cancer cells do not accurately represent the complex cell-cell and cell-ECM interactions that drive cell differentiation, proliferation, gene and protein expression, and especially response to stimuli, and drug metabolism. The use of primary tumor cells from patients can be a good alternative, but the rapid genotypic and phenotypic loss of cells can be another critical issue for applying it to *in vitro* studies [28–30]. Thus, it can be challenging to ascertain the *in vivo* relevance of the findings obtained from models that employ 2D cultured cancer cells as a cellular source.

In this study, we aimed to prepare a suitable cellular source for an *in vitro* cancer extravasation model, by inducing metastatic properties in cancer cells with the pre-culture process. Previous study developed a hydrophobic surface-based spheroid culture platform, which enables the conversion of cancer cells to highly tumorigenic spheroids possessing cancer stem cell (CSC)-like properties, drug resistance to anti-cancer therapeutics, and abundant ECM deposition [31]. Since CSC characteristics are closely associated with metastasis, we investigated the metastatic features of hydrophobic surface-induced cancer spheroid to determine whether they are suitable cellular source for use in metastasis models. Our results showed that cancer cells from hydrophobic surface-induced cancer spheroids exhibit enhanced expression of various extravasation-related genes, aggressive invasion into ECM matrix, and increased endothelial adhesion compared to 2D cultured cancer cells. We then aimed to construct a microfluidic-based *in vitro* extravasation model for investigation of extravasation abilities of 3D cancer cell sources. To achieve this, we designed open-top shaped microfluidic chips produced via 3D printing method, and demonstrated that the microfluidic platform could replicate the interface between cancer cell, endothelial cell, and ECM matrix. We evaluated cancer cell extravasation rates for various surrounding factors, including cytokines and cytokine-secreting cells. Our finding revealed that metastatic cells from hydrophobic surface-induced cancer spheroid showed a much more reactive response to EGF and cytokines secreted from NHLFs and increased extravasation rates compared to 2D cultured cancer cells. These results suggest that different cellular source may regulate their own responses to stimuli in the *in vitro* model, and cancer spheroid induced by hydrophobic surface has high *in vivo* relevancy shown with significant pro-metastatic properties. Furthermore, we identified the cytokines secreted by NHLF and validated the applicability of the constructed model as a drug screening platform for cancer extravasation by treating an inhibitor for identified cytokine, c-c motif chemokine ligand 2 (CCL2). We believe that our proposed platform will serve as a valuable disease model for investigating cancer extravasation and screening potential pharmacological inhibitors.

2. Results and discussion

2.1. In vitro cancer extravasation model using hydrophobic polymer-induced cancer spheroid

Fig. 1 illustrates the production process of an *in vitro* cancer extravasation model that combines a hydrophobic polymer-based cancer spheroid culture platform with a microfluidic-based organ-on-a-chip platform. Initially, cancer spheroids were prepared by culturing cancer cells on hydrophobic surface previously developed [31,32]. The detailed procedure to prepare the hydrophobic cell-culturing surface and cell culture protocol is described in detail in Supporting Information (Fig. S1). Through the pre-culture process for cancer cells, we aimed to enrich cancer cell source with metastatic properties for application to *in vitro* metastasis model. Concurrently, we utilized the 3D printing method to produce a microfluidic chip that can model the extravasation process among various cellular events of metastasis. This chip consists of two main microstructures; an open-top structured collagen gel region where cancer cells metastasize, and a surrounding media channel covered by an endothelial monolayer. The proposed microfluidic chip design enables the construction of hydrogel-endothelium-medium interface without addition of a porous membrane. The height difference between microchannel and open-top region (0.12 mm vs 1 mm) and hydrophobic surfaces prevent leakage of collagen gel into the microchannel during gel loading (Fig. S2). For model preparation, collagen gel harboring chemoattractants, induced by cytokines and cytokine-secreting NHLFs, is first prepared in the center of the chip. The collagen gel type I is a well-known biocompatible material, providing a physiological substrate for endothelial monolayer and parenchymal cells as well as potent space for extravasating tumor cells in the chip [13]. Particularly, the collagen gel remodeling is involved in endothelial monolayer formation during the transendothelial migration of cancer cells during formation of endothelial monolayer is involved in the transendothelial migration of cancer cells [33]. Then, human umbilical vein endothelial cells (HUVECs) are confluently cultured on the

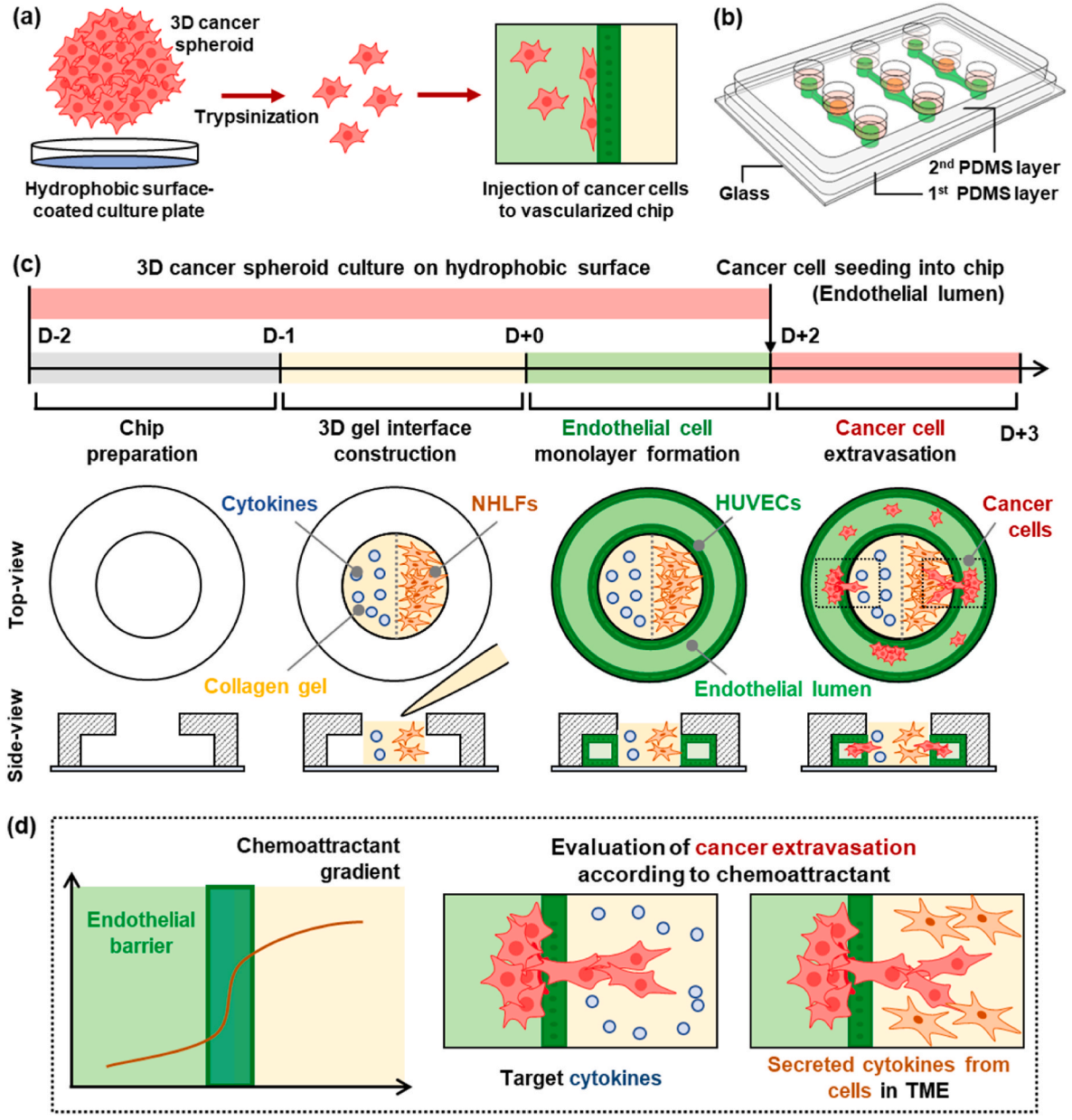

Fig. 1. Schematic illustration of the presented *in vitro* microfluidic model for cancer extravasation utilizing 3D cancer cell sources. (a) 3D cancer spheroids, cultivated on a hydrophobic surface-coated plate to acquire pro-metastatic properties, are subsequently trypsinized into single cancer cells and injected into a vascularized microfluidic chip, where their extravasation rates are evaluated. (b) The microfluidic chip comprises a coverglass and two PDMS layers with microchannels and perforations. These features prevent hydrogel leakage into the microchannel without requiring a porous membrane and facilitate fluid/cell perfusion in the microchannel, serving as medium reservoirs, respectively. (c) The experimental process involves microfluidic chip preparation, the construction of a 3D gel interface using collagen type I hydrogel, formation of an endothelial monolayer, introduction of cancer cells into the endothelial lumen, and the extravasation of cancer cells into the gel toward chemoattractants. The top and side views of the first PDMS layer display the corresponding steps in the process. (d) The microfluidic system is employed to assess the extravasation of 3D cultured cancer cells under a chemoattractant gradient, directed towards the extravascular hydrogel region from the intravascular region. The gradient is established by either adding cytokines or embedding cytokine-secreting cells in the gel region.

hydrogel and polydimethylsiloxane (PDMS) wall surfaces of the media channel to mimic endothelial monolayer of the blood vessel. Finally, pre-cultured cancer cells, enriched with metastatic properties, are seeded inside the media channel surrounded by a HUVEC monolayer. The concentration gradient of cytokines forms toward the endothelial channel where cancer cells are present (Fig. S3). Consequently, the developed microfluidic device can be utilized to determine extravasation rates of cancer cells under pre-metastatic niche with a specific cytokine or parenchymal cells.

2.2. Characterization of metastasis-related key features of hydrophobic polymer-induced cancer spheroids

During metastasis, cancer cells initially leave the primary tumor, invade the stromal-modified spaces, and then enter the blood vessel by penetrating the endothelial barrier, a process known as intravasation [34]. This cellular process involves various changes, including the loss of cell-cell adhesion in the primary tumor, selective migration of cells with stemness and local invasion [35,36]. As a result, the CTCs present in blood vessels after intravasation are a rare tumor cell subpopulation that has acquired metastatic properties [35,37].

Hence, SKOV3 cells, widely used human ovarian cancer cell line for *in vitro* studies, were cultured on the hydrophobic surface-coated culture plate to generate a suitable cellular subpopulation for *in vitro* extravasation study. Previously, we observed the conversion of cancer cells into highly tumorigenic spheroids with CSC-like characteristics, anti-cancer drug resistance, and abundant ECM deposition by culturing them on hydrophobic surface synthesized through initiated chemical vapor deposition (iCVD) process with supplying KnockOut™ Serum Replacement (KOSR) instead of regular FBS in the culture medium [31]. Additionally, our previous study also revealed that these spheroid formation and tumorigenic feature acquisitions were primarily influenced by the adsorption of albumin in the medium to the hydrophobic polymer surface and its structural transformation [32]. Since CSC-like characteristics are closely associated with metastasis, we speculated that such cells would be suitable as a cellular source for a metastasis model. Under four conditions involving two different serums (regular FBS and KOSR) on two different surfaces (TCPS and pV4D4), we observed distinct morphology differences (Fig. 2a, Fig. S4a). Cells cultured with regular FBS on TCPS exhibited typical epithelial-like morphology of SKOV3 cell line, and normal growth. In contrast, cells cultured with KOSR instead of regular FBS on TCPS exhibited an elongated shape with minimal adhesion to the surface, diverging from the original morphology of SKOV3 and notably lower proliferation rates. This led us to conclude that KOSR alone cannot induce spheroid formation and is unsuitable for future applications in extravasation platforms due to low adhesion and proliferation rates. Moreover, when cultured with regular FBS on pV4D4, some cells exhibited a tendency to aggregate each other, while others were observed to adhere to the surface. This indicates that proteins present in regular FBS may play a role in spheroid formation to some extent, but surface alone is insufficient for spheroid formation as well. In contrast, the hydrophobic polymer surface with KOSR induced the formation of spheroids with a relatively uniform size distribution within 4 days (Fig. S4b). These morphological features indicate that combination of hydrophobic polymer surface and choice of serum, KOSR in this study, can induce the formation of spheroids, which is fully consistent with our previous report [31]. We will refer to cancer cells cultured on hydrophobic surface-coated plate or TCPS as 3D source cells or 2D source cells hereafter, respectively.

Key features associated with metastasis of 3D source cell were characterized and compared to those of 2D source cells. Notably, a subpopulation of cancer cells with stem cell-like properties can possess the ability to drive tumor initiation, growth, therapy resistance, and invasion, consequently contributing to cancer metastasis. EMT, the acquisition of mesenchymal features from epithelial cells, is also known to be highly associated with metastasis by inducing the infiltration and metastasizing features during the cancer progression [38]. A number of ligands and receptors, including integrins, cadherins, CD44, and selectins, have been suggested to contribute to adhesion of CTCs to endothelial wall [39,40]. The relative expressions of various genes related to metastasis were evaluated through the quantitative reverse

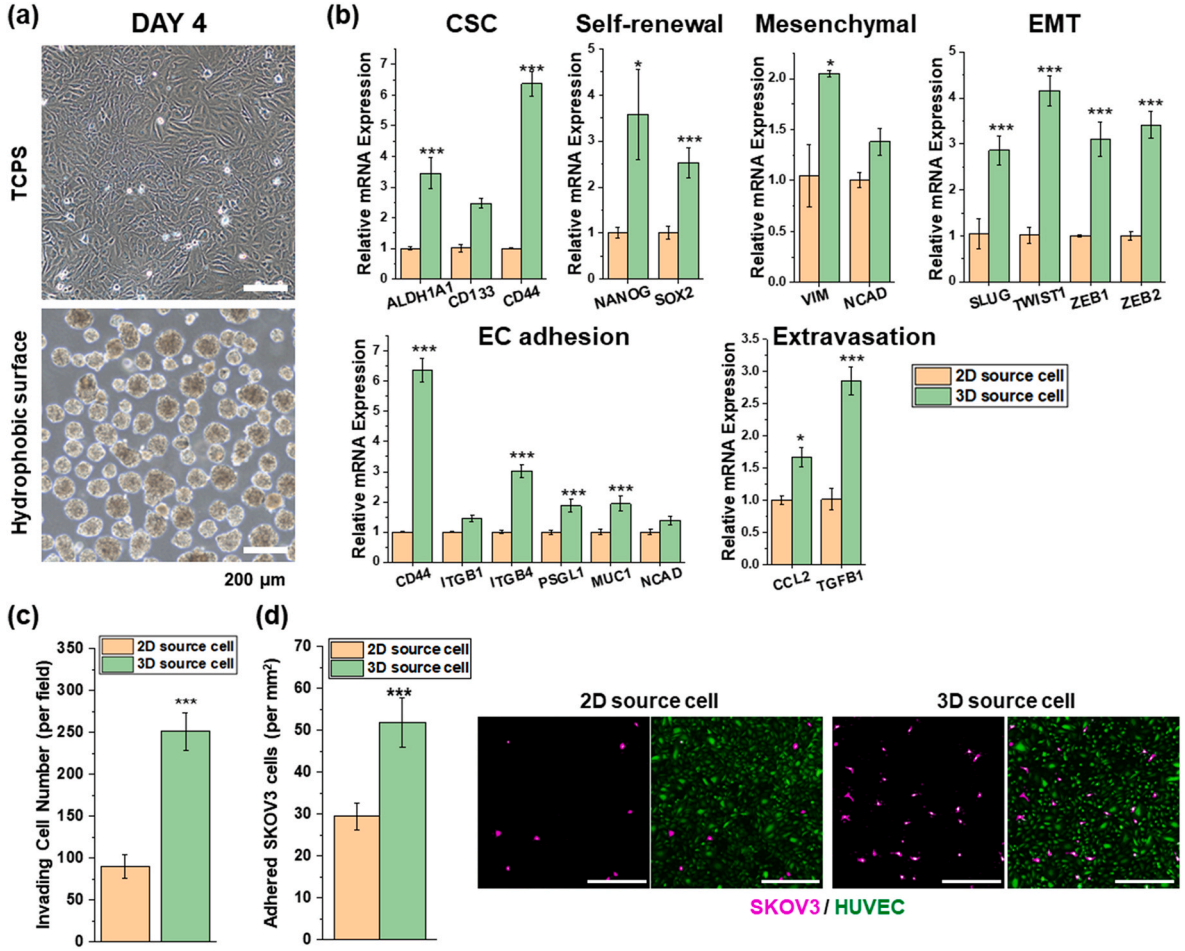

Fig. 2. (a) Morphologies of SKOV3 cells cultured for 4 days on TCPS and pV4D4 (Scale bar = 200 μm). (b) Expression of CSC-associated markers (ALDH1A1, CD133, CD44), self-renewal markers (NANOG, SOX2), EMT-associated markers (VIM, N-CAD, SLUG, TWIST1, ZEB1, ZEB2), Metastasis-associated markers (CD44, ITGB1, ITGB4, PSGL1, MUC1, N-CAD, CCL2, TGFB1) in SKOV3 cells cultured on TCPS and pV4D4, quantified by qRT-PCR ($n = 3$; $^{*}p < 0.05$; $^{**}p < 0.01$, $^{***}p < 0.005$). (c) Quantified number of invaded cells through Matrigel over 24 h ($n = 7$ fields; $^{*}p < 0.05$; $^{**}p < 0.01$, $^{***}p < 0.005$) (d) Representative images and quantified number of adhered SKOV3 cells, cultured on TCPS and pV4D4, on confluent monolayer of HUVEC ($n = 8$ fields; $^{*}p < 0.05$; $^{**}p < 0.01$, $^{***}p < 0.005$). (Scale bar = 200 μm).

transcription polymerase chain reaction (qRT-PCR) analyses including CSC-associated genes (ALDH1A1, CD133, CD44), self-renewal-related genes (NANOG, SOX2), mesenchymal marker genes (VIM, N-CAD), EMT-related genes (SLUG, TWIST1, ZEB1, ZEB2), cancer-endothelial adhesion-related genes (CD44, ITGB1, ITGB4, PSGL1, MUC1, NCAD), and extravasation-related genes (CCL2, TGFB1). All examined genes were upregulated in 3D source cell compared to 2D source cell, suggesting that cancer cells can acquire more metastatic phenotypes through the hydrophobic surface-based cancer spheroid culture platform. Moreover, we conducted a comparison between spheroids generated from ULA plate, one of the most commonly used spheroid culture plates, and hydrophobic surface. The ULA plate has a hydrophilic surface property that significantly suppresses protein adsorption, compelling cells to aggregate and induce the formation of spheroids. Firstly, we observed a notable difference in the size of spheroids cultured on pV4D4 and ULA, even under the same conditions, particularly smaller sizes on pV4D4 (Fig. S4b). Subsequently, we evaluated the relative expressions of various genes associated with metastasis (Fig. S4c). Particularly, 3D source cells from ULA showed no clear trend when compared to 2D source cells, with some genes showing upregulation, while others exhibited similar or even decreased levels of gene expression. Notably, all the examined genes were upregulated in 3D source cells from pV4D4 compared to 3D source cells from ULA, indicating that the spheroids generated on pV4D4 exhibited more

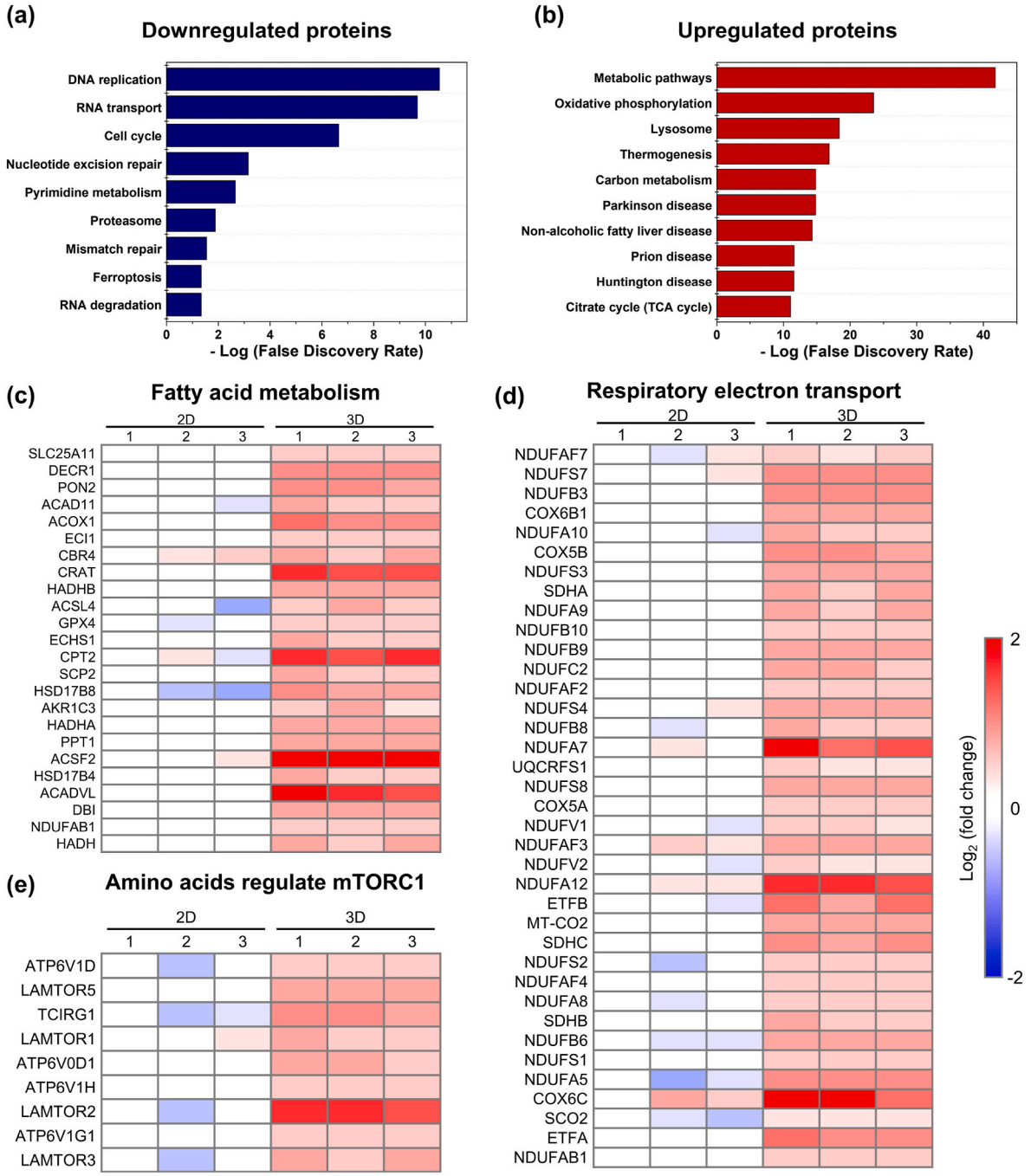

Fig. 3. KEGG pathway analysis showing (a) upregulated and (b) downregulated pathways in 3D source cell compared to 2D source cell. Heatmaps of upregulated proteins in 3D culture cells related to major metabolic pathways including (c) fatty acid metabolism, (d) respiratory electron transport, and (e) amino acids regulate mTORC1.

pro-metastatic features compared to spheroids obtained through conventional methods, even though they displayed spheroid-like cell aggregate morphology. Furthermore, these results strongly suggest that the combinatorial effect of the culture substrate and the choice of serum, rather than KOSR alone, influences not only the morphology but also the pro-metastatic properties.

Next, we conducted several *in vitro* motility assays to confirm the cellular behaviors associated with cancer metastasis. To evaluate the aggressiveness of cancer cells, 2D source cells and 3D source cells were seeded on a Matrigel-coated transwell plate. 3D source cells exhibited a substantial increase in the number of invaded cells compared to the 2D source cells (Fig. 2c). The adhesion of 3D source cells and 2D source cells to endothelial cells was evaluated, by suspending cancer cells on a confluent HUVEC monolayer for 4 h (Fig. 2d). 3D source cells showed a prominent enhancement in the number of adhered cells on HUVEC, regardless of seeding densities. These findings suggest the successful formation of metastatic cancer subpopulation utilizing the hydrophobic surface.

Metastatic cancer cells can exhibit dynamic and selective adaptations in their metabolic pathway to survive metabolic stress in cancerous tissue and advance through metastatic cascade [41]. Therefore, understanding and targeting a distinct metabolic pathway in metastatic cancer is a promising potential therapeutic strategy for mitigating metastasis, and furthermore, related considerations are emerging as one of the important considerations in the *in vitro* modeling [42]. To better understand the distinction between 2D and 3D source cells, we carried out the identification and quantification of the overall protein expressed in each cell source by mass spectrometry-based proteomic analysis [43]. From the results of label-free quantification, 540 upregulated proteins and 504 downregulated proteins were confirmed in 3D source cell compared to 2D ones (Fig. S5a). According to the Kyoto Encyclopedia of Genes and Genomes (KEGG) pathway of differentially expressed proteins (DEPs) in 3D cells, the downregulated proteins were mainly involved in DNA replication, RNA transport, and cell cycle (Fig. 3a). Downregulation of these pathways involved in replication and division has been reported in 3D cultured ovarian cancer cells [44]. On the other hand, the KEGG pathways connected to the upregulated proteins were metabolic pathway, oxidative phosphorylation, carbon metabolism, and TCA cycles (Fig. 3b). Among the metabolic pathways, metabolisms of fatty acid (Fig. 3c), amino acids and derivatives (Fig. S5b), and glucose metabolism (Fig. S5c) were significantly expressed in 3D source cells compared to 2D ones. Displaying diverse metabolic traits is one of the characteristic in metastatic cancer cells [41]. For example, metastatic cancer cells tend to rely on enhanced uptake of glucose, amino acids [45], and fatty acid utilize them as functional signaling molecules and energy sources [46–48]. Cancer cell metabolism has been explained by Warburg effect, which describes that cancer cells can produce energy with enhanced glycolysis in the cytosol and preferential production of lactate, even under the aerobic condition [47,49]. Meanwhile, emerging evidence depicts that diverse metabolic pathways can be activated in the metastatic cascade. Indeed, upregulation of various metabolic processes in cancer cells promotes oxidative phosphorylation through the electron transport system of mitochondria [50–53]. Furthermore, the majority of amino acids have the ability to activate mTORC1 and are controlled by the mTORC1 signaling pathway [45,54]. Both pathway (respiratory electron transport and amino acids regulate mTORC1), shown in Fig. 3d and e, were prominently upregulated in 3D cells versus 2D ones. Previous report confirmed that increased adsorption and secondary structure alternation, α helix-to-β sheet transition, of proteins, particularly albumin, lead to the increase in tumorigenic characteristics through enhanced uptake of albumin in hydrophobic polymer substrate-induced cancer spheroid [32]. Given that albumin can not only be an energy source by itself, but also function as a fatty acids transporter [55,56], we speculate that the amino acid and fatty acid metabolic pathway is activated in hydrophobic-induced cancer spheroids, such as metastatic cancer cells, *in vivo*. Collectively, these results suggest that 3D source cell, prepared on hydrophobic surface-based cancer cell culture platform, exhibit more metastatic metabolic traits compared to 2D source cell.

2.3. Cancer spheroid combined microfluidic-based model capable of confirming the extravasation ability of cancer cells against chemoattractant

Employing the metastatic cancer cells cultivated on a hydrophobic surface, we constructed a microfluidic-based cancer extravasation model possessing interfaces between cancer cells, endothelial cells, and ECM regions, as shown in Fig. 1. Prior to the extravasation assay with microfluidic chips, we examined the EGF-responsive motility of hydrophobic surface-induced cancer cells. We selected EGF as a model chemoattractant, as it has been suggested to induce EMT in cancer cells and promote their motility [57]. We embedded the hydrophobic induced cancer spheroids in collagen type I gel with or without EGF to monitor invasion and EMT state. The EGF-treated spheroids showed a more invasive phenotype and spreaded rapidly than the untreated ones (Fig. 4a). Moreover, vimentin, a mesenchymal marker associated with invasive cancer cells during metastasis, was remarkably pronounced in EGF-treated spheroids (Fig. 4b). These results strongly suggest that hydrophobic surface induced cancer spheroids can acquire mesenchymal features and invasiveness as aggressive cancer cells separate from the primary tumor by losing their cell-cell junctions and invade to stromal modified spaces, under the chemoattractant cue [3].

Next, the extravasation ability of 2D source cell and 3D source cell against the EGF gradient was assessed using vascularized microfluidic chips (Fig. 4c). After dissociating the spheroids into dispersed cancer cells, we introduced the cancer cells into chip reservoirs that were connected to intravascular regions, and observed cancer extravasation toward collagen gel containing EGF. The extravasation rates were less than 12% for the 2D source cell regardless of presence of EGF, showing no significant difference. In contrast, the extravasation rate was nearly 20% for the 3D source cell, significantly higher than that of 2D source cell even without EGF supplement, and increased by about 1.7-fold when the EGF gradient was formed in the chip (Fig. 4d and e). The confocal imaging confirmed that cancer cells extravasated between cell junctions of confluently cultured HUVEC monolayer (Fig. 4f, Fig. S6). In case of 2D source cell, only a few cancer cells could adhere to the inside of HUVEC monolayer, and even the attached cells hardly cross the endothelial barrier. On the other hand, in case of metastatic 3D source cell, a large number of cells were adhered to the HUVEC, and extravasated through the junction of the endothelial barrier within 24 h. In addition, disruption of cell junctions of HUVEC (vascular endothelial cadherin; VE-cadherin) was also confirmed at the sites of transendothelial migration of 3D source cells, which can be regarded as a direct evidence of extravasation (Fig. 4g). Real-time imaging of cellular events is one of the unique advantageous features of microfluidic-based chips, allowing direct and in-situ observation of specific cellular behaviors. The detailed sequence of extravasation of metastatic 3D source cell under the EGF gradient was observed by real-time imaging (Fig. S7, Supporting video V1). Cancer cells could adhere onto HUVEC monolayer within first 3 h, and migrate through the cell junctions of HUVECs 6 h after injection, and eventually invade to the collagen gel region according to the chemoattractant gradient. These findings highlight the heightened sensitivity of metastatic 3D source cells to EGF compared to 2D source cells. Furthermore, it's noteworthy that the potential under- or overestimated results obtained from 2D source cells can be adjusted by employing 3D source cells, indicating that 3D source cells are a suitable cellular source for *in vitro* cancer extravasation model.

Supplementary video related to this article can be found at https://doi.org/10.1016/j.bioactmat.2023.12.021

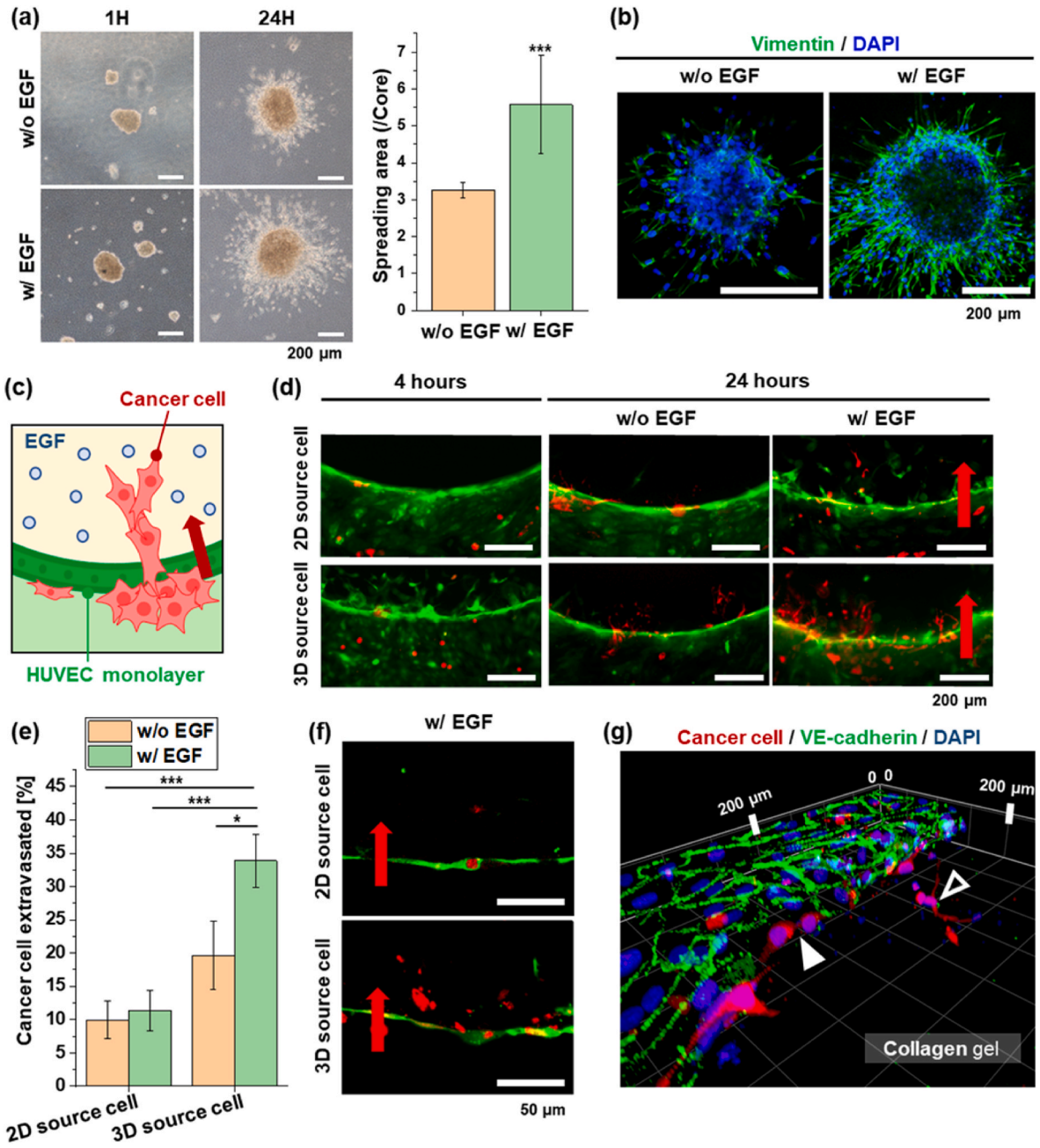

Fig. 4. Comparing extravasation rates of 3D and 2D cancer cells in response to EGF as a chemoattractant. (a) Representative images showing the invasion of cancer spheroids embedded in collagen I gel over 1 and 24 h with or without EGF (Scale bar = 200 μm), and quantified data ($n = 8$, $^{*}p < 0.05$; $^{**}p < 0.01$, $^{***}p < 0.005$). (b) Immuno-fluorescence images showing the expression of vimentin (green) and nucleus (blue) in the cancer spheroids 24 h after embedding in collagen I gel with or without EGF (Scale bar = 200 μm). (c) Illustration of the constructed interface of HUVEC, cancer cell, and EGF in the chip model. (d) Representative images showing the extravasation of 2D source cancer cells and 3D source cancer cells (red) through the HUVEC layer (green) over 28 h with or without EGF in the chip model (Scale bar = 200 μm), and (e) quantified data ($n > 7$ chips, $^{*}p < 0.05$; $^{**}p < 0.01$, $^{***}p < 0.005$). (f) Confocal images showing the extravasation of 2D source cancer cells and 3D source cancer cells (red) through HUVEC (green) over 24 h with EGF gradient (Scale bar = 50 μm). (g) 3D reconstruction of confocal image showing the 3D source cancer cells (red), expression of VE-cadherin (Green) of endothelial monolayer, and Nucleus (blue) at the moment of extravasation with EGF gradients. Filled and empty white arrows indicate extravasating cancer cells through disruption of endothelial junctions and fully extravasated cancer cells in the matrix, respectively.

2.4. Cancer spheroid combined microfluidic-based model capable of confirming the extravasation ability of cancer cells against cytokine-secreting cells

The open-top design of microfluidic system enables the quantitative evaluation of guidance roles of cytokine-secreting parenchymal cells on extravasation potential of cancer cells. Fibroblasts are one of the most prevalent and significant elements during metastasis in both primary tumors and metastatic sites, and they can secrete a variety of cytokines to promote tumorigenesis [58]. Prior to the on-chip extravasation assay, we aim to validate NHLF-responsive invasion of hydrophobic surface-induced cancer cells in 3D hydrogel. Hydrophobic surface-induced cancer spheroids were embedded in collagen I gel with or without NHLF-conditioned medium to monitor the invasion and EMT state. Spheroids treated with NHLF-conditioned medium displayed a more invasive phenotype and larger spread area (Fig. 5a). Furthermore, invasive cells from NHLF media-treated spheroids showed pronounced expression of vimentin (Fig. 5b). These results further imply that

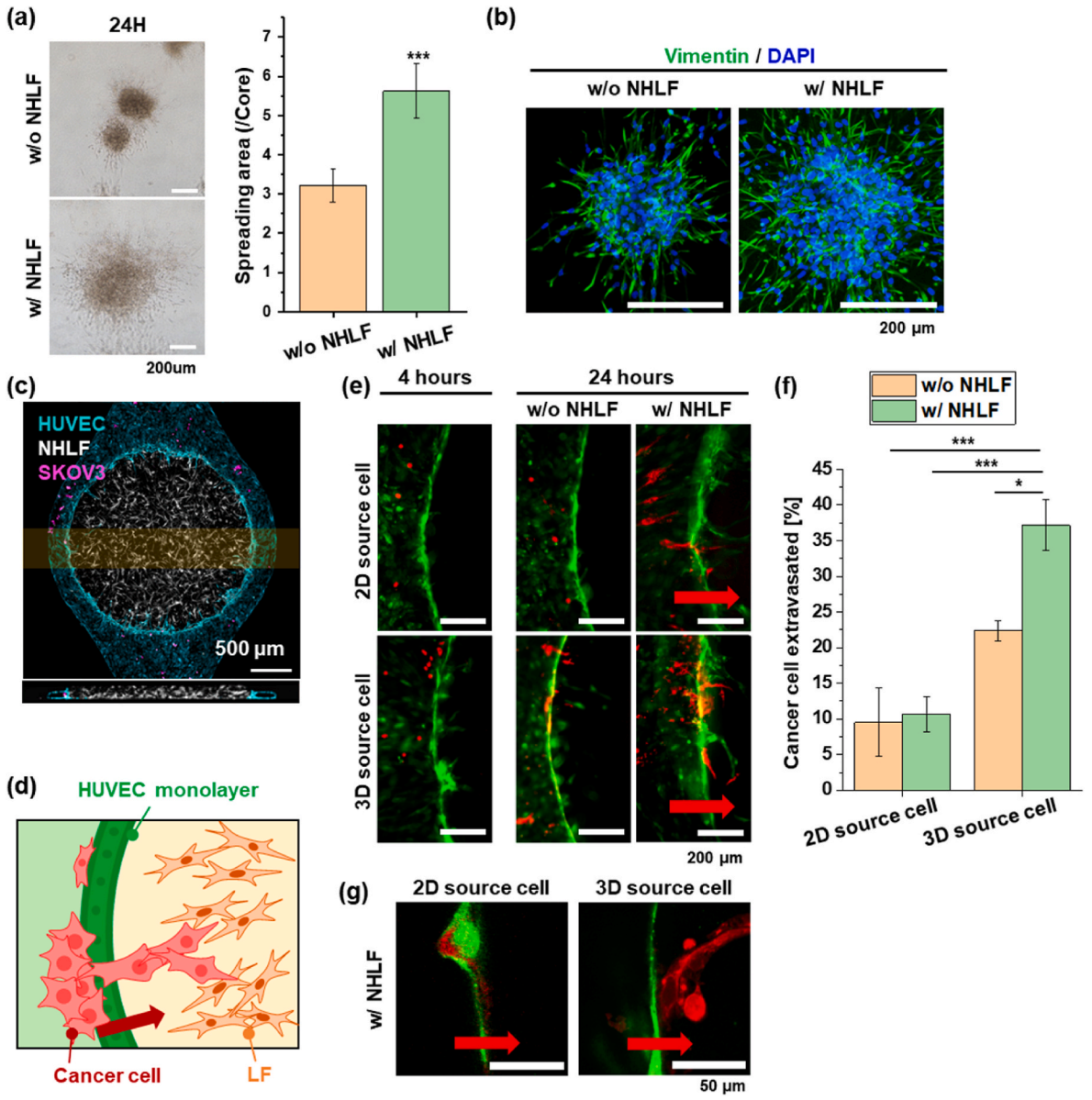

Fig. 5. Comparing extravasation rates of 3D and 2D cancer cells in response to cytokine-secreting NHLFs. (a) Representative images showing the invasion of cancer spheroids embedded in collagen I gel over 24 h with or without conditioned medium from NHLF (Scale bar = 200 μm), and quantified data ($n = 8$, $^{*}p < 0.05$; $^{**}p < 0.01$, $^{***}p < 0.005$). (b) Immuno-fluorescence images showing the expression of vimentin (green) and nucleus (blue) in the cancer spheroids 24 h after embedding in collagen I gel with or without conditioned medium from NHLF (Scale bar = 200 μm). (c) Visualization of fabricated extravasation model chip showing the location of each cell, HUVEC (cyan), SKOV3 (purple), and NHLF (White) (Scale bar = 500 μm). (d) Illustration of the constructed interface of HUVEC, cancer cell, and NHLF in the chip model. (e) Representative images showing the extravasation of 2D source cancer cell and 3D source cancer cell (red) through the HUVEC layer (green) over 24 h with or without NHLF in the chip model (Scale bar = 200 μm), and (f) quantified data ($n > 3$ chips, $^{*}p < 0.05$; $^{**}p < 0.01$, $^{***}p < 0.005$). (g) Confocal images showing the extravasation of 2D source cancer cell and 3D source cancer cell (red) through HUVEC (green) over 28 h with NHLF (Scale bar = 50 μm).

hydrophobic surface induced cancer spheroids respond sensitively to chemoattractant cues, and develop invasiveness while undergoing EMT.

To further study the chemoattractive interactions between parenchymal and cancer cells within microfluidic chips, NHLFs were seeded with the collagen in the center hydrogel region. A side-view confocal image also confirmed the formation of confluent HUVEC monolayer and the uniform distribution of NHLF in the collagen gel (Fig. 5c). Then, the extravasation rates of 2D source cancer cell and 3D source cancer cell against NHLF-secreting cytokines were analyzed (Fig. 5d, Fig. S6). The extravasation rate of 2D source cells was less than 11%, regardless of the presence of NHLF, whereas the extravasation rate of 3D source cells was almost 23% even without NHLFs, which was significantly increased by about 1.6-fold in the presence of NHLFs (Fig. 5e and f). Confocal imaging showed much enlongated morphology of 3D source cell toward NHLFs-embedded collagen gel compared to 2D cell, which provides a basis for the higher extravasation rates of the 3D source cells (Fig. 5g). Taken together, these observations suggest that metastatic 3D source cells show highly responsive motility to cytokines that are secreted from tissue cells, implying that more physiological assay is applicable by utilizing the parenchymal cells found in secondary site of extravasation.

2.5. *On-chip investigation of pharmacological inhibitions of CCL2-mediated cancer cell extravasation*

In the aforementioned sections, we presented the *in vitro* extravasation system by integrating the hydrophobic surface induced 3D cancer cell source to microfluidic-based disease model. Our model allowed the quantitative evaluation of extravasation ability of engineered pro-

metastatic cancer cells under chemotactic gradient made by introducing a cytokine cue or cytokine-secreting cells in the adjacent collagen gel, providing adequate microphysiological testbed in regards to reconstitution of metastatic microenvironment at secondary site *in vivo* counterpart. On the basis of the results, we further aimed to identify whether a specific soluble protein among NHLF-secreting cytokine repertories is responsible for the pro-extravasating behaviors of 3D cancer cell sources. This investigation can rationalize the applicability of the constructed *in vitro* model as a drug screening platform for cancer extravasation. When a specific cell-cell interface is formed in the model, the simple microfluidic platform could be operated for screening potential drug targets as below: profiling of secreted cytokines, pharmacological blockage of a candidate cytokine, and evaluation of cancer extravasation rate under inhibition (Fig. 6a).

Employing the approach above, we first identified the putative cytokines involved in the cancer extravasation using a cytokine array against NHLF-conditioned medium. Semi-quantitative analysis for NHLF-conditioned medium indicated that the expressions of various cytokines increased in NHLF culture compared to base medium, particularly Tissue inhibitor of metalloproteinases 2 (TIMP-2), CCL2, and Osteoprotegerin (OPG) with higher extent (>8-fold) (Fig. 6b, Fig. S8). Among the highly secreted cytokines, we investigated the effects of therapeutic inhibition of CCL2 on cancer cell extravasation. The CCL2 (also known as monocyte chemoattractant protein 1; MCP-1), highly expressed by host tissue cells, facilitates not only recruitment of monocytes but also migration and progression of tumor cells such as breast [17,59,60], ovarian [61,62], prostate [63], and bladder cancer cells [64]. Of note, the NHLFs showed remarkable expressions of CCL2 unlike previous study where CCL2 was non-detectable from normal human dermal fibroblast-conditioned media [65]. To block the binding interactions between soluble CCL2 secreted by NHLFs and CCR2 expressed by cancer cells, we introduced the cancer cells into a microfluidic channel with CCL2 neutralizing antibody, and incubated the chips under the CCL2 inhibitors for 24 h. As a result, extravasation rate of 3D source cells was significantly reduced with increasing doses (22% at 2.5 μg/mL anti-CCL2 v.s. 44% at IgG control), compared to that of 2D source cells (13% at 2.5 μg/mL anti-CCL2 v.s. 7% at IgG control) (Fig. 6c and d). Interestingly, 2.5 μg/mL anti-CCL2 induced the reduction of extravasation rate similar to that of condition without NHLF (Fig. 5f).

Despite notable expressions of TIMP-2 and OPG, we focused on CCL2 due to its relevance in our model given the previous studies. Ovarian tumor cells, along with the surrounding stromal cells, induce the synthesis or activation of a group of proteolytic enzymes referred to as MMPs, aiming to support tumor growth, invasion, and eventual metastasis [66,67]. Consequently, any disruptions in the balance between MMPs and their inhibitors, TIMPs, dictate the nature of the tumor

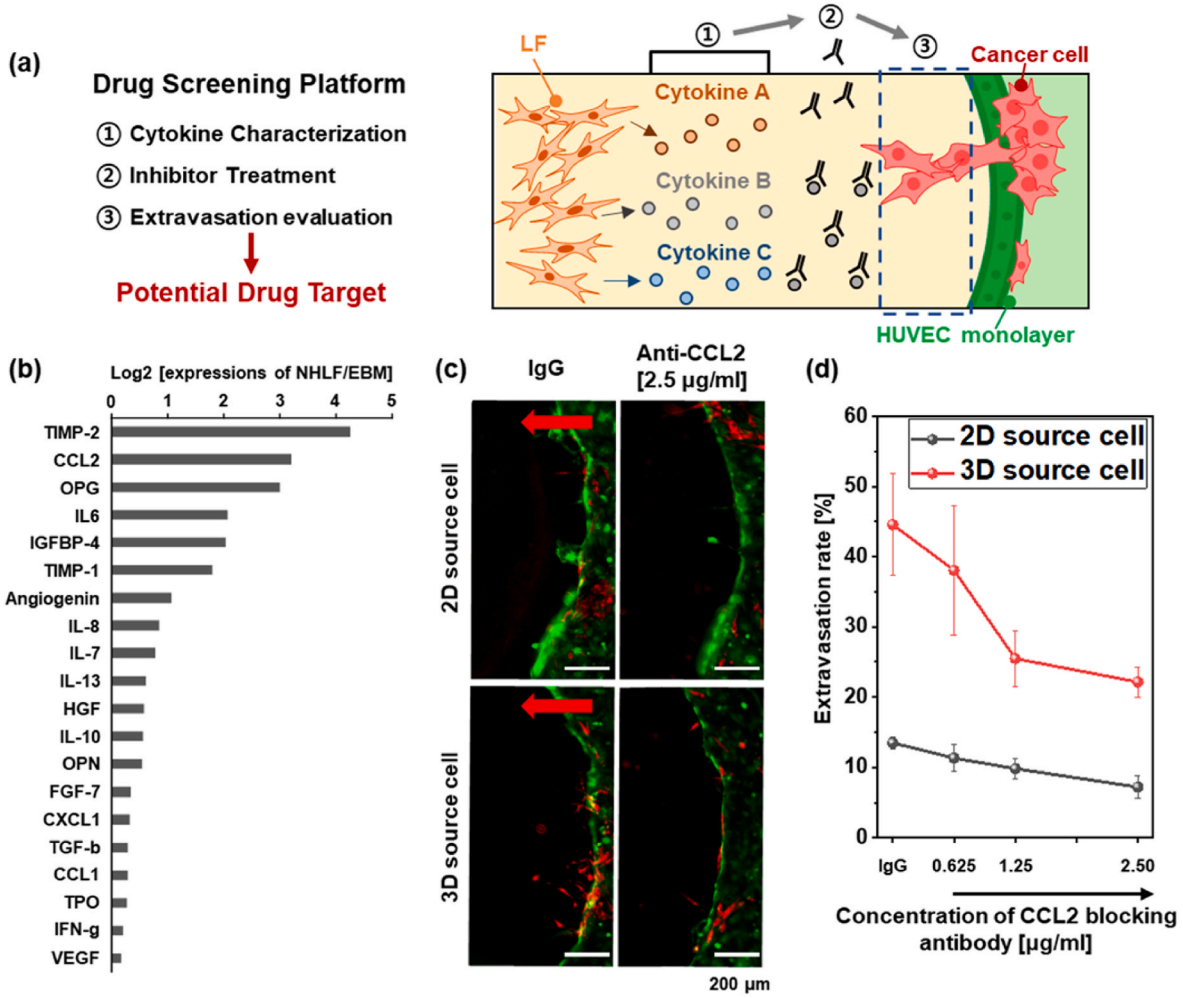

Fig. 6. Pharmacological inhibitions targeting CCL2-mediated extravasation of 3D cancer cells. (a) Schematic illustration of the process in which the extravasation model is used as drug screening platform. (b) Top 20 relative expressions of cytokines in the NHLF-conditioned medium over basal medium are shown (n = 3). All expressions of 80 proteins analyzed by the cytokine array are shown in Fig. S8. (c) Representative images showing the extravasation of cancer cell (red) through the HUVEC layer (green) over 28 h with NHLF, and with or without anti-CCL2 in the chip model (Scale bar = 200 μm), and (d) quantified data ($n > 3$ chips, $^{*}p < 0.05$; $^{**}p < 0.01$, $^{***}p < 0.005$).

microenvironment, potentially facilitating metastasis. Despite the noticeable expression of TIMP-2 from the NHLF-conditioned medium in our findings, it is plausible that the MMP expressions by the SKOV3 cells might overshadow TIMP-2, leading to the deterioration of the surrounding hydrogel following the disruption of endothelial junctions. Another remarkable cytokine in the NHLF-conditioned medium, OPG, is known to bind to the receptor activator of nuclear factor-kB ligand (RANKL), thereby inhibiting osteoclastic bone resorption and being involved in bone remodeling [68]. OPG also participates in cancer-induced bone degradation, where it shields prostate cancer cells from the apoptotic effects of TRAIL, offering survival advantages to tumor cells [69]. We speculate that TIMP2 and OPG may have some effect on the increased extravasation rates of 3D cancer cells compared to 2D one, which requires further extended research.

Taken together, these results suggest a potential application of our microfluidic disease model with 3D metastatic cell sources as a anti-metastatic drug screening platform. Considering the underlying complex mechanisms in the metastasis process *in vivo* and growing evidences for microfluidic system as a standardized disease model *in vitro*, we belive that our integrative approach rationalize the improvement to current microphysiological systems and the contribution for a potential strategy for anti-metastatic drug screening.

3. Conclusion

In this study, we have suggested the critical importance of the characteristics of the cancer cellular source in constructing an *in vitro* metastasis model with *in vivo* relevancy. Using hydrophobic surface-based spheroid culture platform, we could induce the conversion of 2D cultured cancer cells to highly pro-metastatic spheroids exhibiting aggressiveness, adhesion ability to endothelial cells, and activated metabolic traits. Subsequently, we developed an *in vitro* extravasation model by integrating the engineered pro-metastatic cancer cells with a microfluidic chip where cell-to-cell 3D interfaces were constructed. As a result, metastatic cells from hydrophobic surface-induced spheroids exhibited increased extravasation rates and were significantly reactive to EGF and cytokines secreted from NHLF compared to 2D cultured cancer cells. This suggests that meaningful experimental results with high *in vivo* relevancy can be accurately acquired using 3D source cells, overcoming potential oversights associated with conventional 2D source cells. The microfluidic-based model, with its real-time capabilities and immunocytochemistry analysis provides a unique advantage for detailed observation of the extravasation process. Furthermore, the study validated the applicability of the microphysiological model as an anti-metastasis drug screening platform through cytokine profiling and therapeutic inhibition. We believe that our extravasation model could be applied to basic metastasis research and potential drug development process.

4. Experimental section/methods

4.1. Synthesis of hydrophobic surface-coated culture plate via the iCVD process

Poly(2,4,6,8-tetravinyl-2,4,6,8-tetramethyl cyclotetrasiloxane) (pV4D4) polymer was selected to create hydrophobic surface-coated culture plate as previously reported [31,70]. pV4D4 polymer film was synthesized and simultaneously deposited directly onto culture substrate through iCVD process. Vaporized V4D4 monomer and the initiator, *tert*-butyl peroxide (TBPO), were introduced into the iCVD reactor with flow rates of 1.489 and 2.093 sccm, respectively. V4D4 was heated to 70 °C for the vaporization, whereas TBPO was not heated. The pressure of the chamber was maintained to 280 mTorr, and the filaments in the iCVD reactors were heated to 140 °C. For the adsorption of monomers, the temperature of the cooling stage was set to 38 °C. The deposition rate of the polymer film was about 2.5 nm/min. The detailed characterization methods and results were described in Supporting information (Fig. S1).

4.2. Cell culture conditions and cancer spheroid formation

SKOV3 cells were cultured in RPMI-1640 medium (Gibco) supplemented with 10% (v/v) fetal bovine serum (FBS; Gibco), 1% (v/v) penicillin/streptomycin (P/S; Gibco), and 25 mmol/L HEPES (Gibco). For inducing formation of cancer spheroid, SKOV3 cells were seeded on the pV4D4-coated culture plate in RPMI-1640 medium containing 10% (v/v) KnockOut™ Serum Replacement (KOSR; Gibco), 1% (v/v) penicillin/streptomycin (P/S; Gibco), and 25 mmol/L HEPES (Gibco) with the seeding density of 1.0×10^5 cells/mL. All the cells and spheroids were cultured at 37 °C in a humidified 5% CO_2 atmosphere. The culture medium was replaced every two days, and cells were imaged after 48 and 96 h of seeding using optical microscopy (Ti–U, Nikon). In some experiments, cell tracker was labeled with cell tracker (CellTracker™ Red (CTR) CMTPX Dye, invitrogen) for the visualization of SKOV3 cells. Briefly, single cells were suspended in serum-free RPMI with the density of 2000 cells per microliter and stained for 45 min with 5 μM of CTR at 37 °C in a humidified 5% CO_2 atmosphere. Human umbilical vein endothelial cells (HUVECs, Lonza) and HUVECs transfected with green fluorescence protein (GFP-HUVECs, Angio-Proteomie) were cultured in EGM-2MV (Lonza) supplemented with 1% (v/v) P/S. Normal human lung fibroblasts (NHLFs, Lonza) were cultured FGM-2 (Lonza) supplemented with 1% (v/v) P/S. Only four to seven passages of HUVECs and NHLFs were used in the experiments. All cells were maintained at 37 °C in a humidified 5% CO_2 atmosphere.

4.3. qRT-PCR

Total RNA of cells was isolated according to the manufacturer's instructions (RNeasy Mini kit; Qiagen). The RNA was reverse transcribed into cDNA according to the manufacturer's instructions (cDNA synthesis kit; Toyobo) by using T100 thermal cycler (Biorad). qRT-PCR analyses of various genes (ALDH1A1, CD133, CD44, SOX2, NANOG, VIM, N-CAD, SLUG, TWIST1, ZEB1, ZEB2, ITGB1, ITGB4, PSGL1, MUC1, CCL2, TGFB1) were performed according to the manufacturer's instructions (SYBR green real-time PCR master mix, Toyobo) by using CFX96 Real-time PCR detection system (Bio-Rad), while β-actin were used as housekeeping genes. Primers used in this study (GenoTech Corp) were listed in Table S1.

4.4. Transwell migration assay

SKOV3 cells cultured on TCPS and cancer spheroids cultured on pV4D4 were starved in the serum-free medium for 24 h and dissociated into single cells using trypsin before starting the assay. Then, cells were seeded on the top of the filter membrane (PET, 8.0 μm pore size) coated with Matrigel (200 μg/mL, Corning) in a transwell insert (1.0×10^4 cells/well). After filling the medium containing 10% FBS into the lower chamber, cells were incubated for 24 h to induce the invasion of cells through the matrigel-coated membrane. Then, cells were fixed with 4% formaldehyde (Sigma). Non-invaded cells on the upper chamber of the membrane were removed by using a cotton swab. The remaining cells on the lower surface of the membrane were stained with DAPI and counted using inverted fluorescent microscopy (Ti–U, Nikon). The number of invaded cells was averaged per seven random fields on each membrane using the ImageJ software (NIH).

4.5. Adhesion of cancer cells on 2D cultured endothelial cell

HUVECs were seeded on the cell culture plate and cultured until a confluent monolayer. Then, cancer cells, which were from TCPS or dissociated from pV4D4-induced spheroid, were labeled with CTR and seeded on the confluent HUVEC layer as cell suspensions with the

seeding density of 1.0×10^4 cells/mL. After incubating the cells for 4 h and wahsing the cells three times, adhered cancer cells were counted using inverted fluorescent microscopy (Ti–U, Nikon) to evaluate the adhesion ability of cancer cells. The number of adhered cells was averaged per eight random fields on each membrane using the ImageJ software (NIH).

4.6. Microfluidic chip fabrication and on-chip endothelial monolayer formation

Poly-dimethyl-siloxane (PDMS, Dow Corning) microfluidic chips were fabricated using a 3D-printed SLA mold. In brief, using the SolidWorks program (Dassault Systèmes), we first designed two types of molds for fabricating two PDMS layers of chip, such as microchannel-engraved layer and reservoir-perforated layer. The microchannel layer has a central hole with 2-mm-diameter, a surrounding microchannel with cross-sectional dimensions of 350-μm-width and 120-μm-height, and two 2-mm-diameter holes connected to the microchannel. The reservoir layer has three 4-mm-diameter holes whose centerpoints coincide with the holes of the microchannel layer. A 3D-printed SLA mold was produced from the design (CEP Tech, Rep. of Korea). After mixing PDMS base and its curing agent at a ratio of 10:1.5 (w/w), the mixture was poured onto the molds, degassed with vacuum pump for 30 min, and cured at 55 °C for 4 h. After perforating reservoirs with biopsy punch, the PDMS were sterilized by 15 min ultrasonication in 70% (v/v) ethyl alcohol. The sterilized PDMS layers were bonded to a cleaned 1.0 H-thickness cover glass (DWK lifescience) after being exposed to ambient air plasma (Femto Science). To enhance hydrogel adhesion, the chips were coated with polydopamine solution at concentration of 8 mg/mL in 10 mM Tris-HCl for 2 h under the UV ray. Then, the chips were washed twice with distilled water and left in the 75 °C oven at least 48 h to recover the surface hydrophobicity.

Collagen gel (pH 7.4, 2.5 mg/mL) was prepared with type I collagen gel from rat tail (Corning), distilled water, 10X PBS, and 0.5 N NaOH on an ice bucket. If needed, trypsinized NHLF cells were mixed with the collagen gel at a final concentration of 5×10^5 cells/mL. The 8 μL of gel mixture was introduced to the open-top central region of the PDMS chip, and incubated for 60 min in the humidified 37 °C 5% CO_2 atmosphere. After filling the surrounding microchannel with 300 μg/mL Matrigel in serum-free EBM, the chips were incubated for 45 min, washed gently with EGM-2MV, and kept in the 37 °C 5% CO_2 incubator. Next day, HUVECs were washed, detached, and prepared to a final concentration of 3×10^6 cells/mL with PBS, EDTA-trypsin (0.25% w/v), and EGM-2MV, respectively. Then, HUVECs suspension was injected into the one of the reservoirs of the microchannel and the chips were incubated for 1 h at humidified 37 °C 5% CO_2 and unbound cells in the microchannel were washed with EGM-2MV. The chips containing gel and cells were further incubated for 48 h with daily replenishment of EGM-2MV until the HUVECs grow and cover the all surfaces of gel-microchannel.

4.7. Monitoring and quantification of extravasation

Before seeding cells into the chip, SKOV3 cells cultured on TCPS and cancer spheroids cultured on pV4D4 were dissociated into single cells using trypsin. For the visualization of SKOV3 cells, cells were pre-labeled with CTR and Hoechst 33 342 (1 μg/mL) as described above. The cells were prepared with EGM-2MV at concentrations of 8×10^4 cells/mL. Then, the SKOV3 cells was injected into the reservoir and flowed in the microchannel and the chips were incubated for 4 h in a humidified 37 °C 5% CO_2. The applied pressure difference (8 mmH_2O) between the reservoirs and central open-top region allowed the suspending cancer cells to tend to attach to the HUVEC monolayer. The chips were further cultured for 20 h with addition of EGM-2MV media (if needed, containing EGF or inhibitors) in the reservoirs.

After total 24 h of incubation, the chips including NHLF, GFP-HUVECs and CTR-SKOV3 were imaged with epi-fluorescence microscope (Axio Observer Z1, Carl Zeiss) with an objective (EC Plan-Neofluar 10x/0.30 Ph 1). If needed, epi-fluorescence images of extravasating SKOV3 cells were obtained within a 37 °C 5% CO_2 live-imaging chamber. The cells were then fixed, permeabilized, and washed with PFA (4% w/v in PBS) for 15 min, Triton X-100 (0.5% v/v in PBS) for 20 min, and PBS, respectively. Some sites of SKOV3 extravasation were imaged as 3D stacks using a confocal microscope (Axio Observer LSM 880, Carl Zeiss) with 1.4-μm-interval with an objective (Plan-Apochromat 20x/0.8 M27). After processing the images with ZEN (Carl Zeiss) or ImageJ software, the fully-extravasated or non-extravasated SKOV3 cells were counted over the entire chip and the extravasation percentage was quantified.

For blocking CCL2-CCR2 binding interactions, the cancer cell suspensions were supplemented with anti-CCL2 antibody (R&D Systems, 2.5 μg/mL) and then introduced into one of the microfluidic chip reservoirs that connected to the intravascular region. The microfluidic chips were incubated 4 h in a humidified 37 °C 5% CO_2, and further culture for 20 h with addition of EGM2-MV containing anti-CCL2 antibody.

4.8. Cytokine array

To compare relative secretion of cytokines from NHLF cells, the conditioned-media sample from NHLF cells were analyzed using a cytokine array (Human Cytokine Antibody Array C5, RayBiotech). In brief, confluent NHLF cells in a 60-mm-dimater plate were incubated with EBM for 24 h, and the conditioned-media was harvested and stored at −70 °C until use. For negative control, NHLF cells were omitted from the plate. According to the manufacturer's instructions, the collected conditioned media was centrifuged at 3000×*g* for 5 min and incubated with multiple membranes. Then, the membranes were incubated with biotinylated antibody cocktails and labeled streptavidin. The resulting membranes were scanned using a chemiluminescence imaging system (ChemiDoc, Bio-Rad Laboratories) and their spot signal densities were processed using Protein Array Analyzer plugin in ImageJ software for quantification.

4.9. Sample preparation for proteomics

Add 300 μl of a 0.2% DDM solution containing 150 mM NaCl, 50 mM Tris-HCl, and one protease tablet to the cell pellets in order to extract the protein from SKOV3, and then lyze the cells at 95 °C for 10 min after mixing. In order to eliminate cell debris and collect the supernatants, the mixture was centrifuged at 12 000×*g* for 15 min. From the BCA test, the total protein concentration in the isolated proteins was determined.

A 50 mM Ambic solution containing 10 mM DDT was used to denaturize 10 μg of protein. 40 nM IAA was added to protein sample and reacted at room temperature for 30 min to stop the disulfide bond formation from folding back together. After that, the mixture was treated with trypsin (protein:enzyme = 20:1) and digested for 18 h at 37 °C to break down the protein as peptide. The peptide solution was purified using an HLB cartridge and then dried. The dried samples were frozen at −20 °C before nano-flow liquid chromatography-electrospray ionization-tandem mass spectrometry (nLC-ESI-MS/MS).

4.10. NanoflowLC-ESI-MS/MS analysis

The dried samples were reconstituted in a solution of H_2O:ACN (98:2, v/v) containing 0.1% FA, and 250 ng of the resulting peptide mixture were introduced into a NanoElute LC system connected to a hybrid trapped ion mobility spectrometry-quadrupole time-of-flight mass spectrometer (timsTOF Pro, Bruker Daltonics, Bremen, Germany), equipped with a modified nano-electrospray ion source (CaptiveSpray, Bruker Daltonics). The peptide mixtures were separated at 50 °C with a constant flow of 400 nL/min on a handmade column (75 μm-inner diameter, 250 mm-length) packed with C18 resins (1.9 μm, 120, Dr.

Maisch), and they were eluted using the following binary gradient of mobile phases A (0.1% FA in H2O) and B (0.1% FA in ACN): 2%–17% B for 45.0 min, 17%–25% for 22.5 min, 25%–37% for 7.5 min, 37%–80% for 5.0 min, and then kept at this level for 10 min to rinse the analytical column. Bruker Compass Hystar 5.0.37.1 was used to operate the timsTOF Pro in the parallel accumulation serial fragmentation (PASEF) acquisition mode. The following settings were used for MS and MS/MS scans: mass range of 100–1700 m/z, $1/K_0$ start at 0.6 Vs/cm^2 and end at 1.6 Vs/cm^2, capillary voltage of 1500 V, dry gas flow rate of 3 L/min, and dry temperature of 180 °C; PASEF mode: 10 MS/MS scans (total cycle time 1.16 s), charge range of 0–5, active exclusion for 0.4 min, scheduling target intensity of 20 000, intensity threshold of 2500, depending on precursor mass and charge.

4.11. Data analysis

For protein identification and label-free quantification (LFQ) searches against the SwissProt database of Homo sapiens (human, UP00000564, downloaded 22/11/2019, 20 379 entries) from Uniprot (www.uniprot.org), the obtained raw data were submitted to PEAKS Studio 10.5 (Bioinformatics Solutions, Waterloo, Canada) with a false discovery rate (FDR) of 0.01. The following were the search parameters for identification: trypsin is the required enzyme, and two missed cleavages are allowed. Additionally, there are the following modifications: (a) carbamidomethylation of cysteine is a fixed modification, and (b) methionine oxidation and acetylation of the protein N-terminus are variable modifications that allow for three different PTMs per peptide. After the protein identification process was finished, LFQ was carried out using the analyzed PEAKS dataset. The LFQ analysis was performed using the analysis of variance (ANOVA) method, and the thresholds for significance were two unique peptides, a data filter in at least two samples per group, a significance of 13 (p-value = 0.05), and a 1.5-fold change. Data normalization was carried out using total ion chromatography (TIC). After the data were exported to Microsoft Excel, the STRING (version 11.5) was used to perform KEGG pathway analysis and reactome pathway enrichment on the dataset.

4.12. Statistics

All data are reported as mean ± standard error of mean. Statistical analysis was performed with OriginPro software (OriginLab) using the two-sample *t*-test when comparing two conditions or one-way ANOVA followed by Tukey multiple comparison test when applicable. All tests with $p < 0.05$ were considered to be statistically significant. The measurements were obtained from more than three independent samples.

Statement of ethics

This study doesn't include clinical experiment, animal experiment, and human subjects.

CRediT authorship contribution statement

Minseok Lee: Conceptualization, Data curation, Formal analysis, Investigation, Methodology, Validation, Visualization, Writing – original draft, Writing – review & editing. **Seunggyu Kim:** Conceptualization, Data curation, Formal analysis, Investigation, Methodology, Validation, Visualization, Writing – original draft, Writing – review & editing. **Sun Young Lee:** Formal analysis, Investigation, Methodology, Writing – original draft, Writing – review & editing. **Jin Gyeong Son:** Formal analysis, Investigation, Methodology, Writing – original draft, Writing – review & editing. **Joonha Park:** Investigation, Methodology, Visualization, Writing – original draft, Writing – review & editing. **Seonghyeon Park:** Investigation, Methodology, Validation, Writing – original draft, Writing – review & editing. **Jemin Yeun:** Investigation, Writing – original draft, Writing – review & editing. **Tae Geol Lee:** Funding acquisition, Project administration, Resources, Supervision, Writing – original draft, Writing – review & editing. **Sung Gap Im:** Conceptualization, Funding acquisition, Project administration, Resources, Supervision, Writing – original draft, Writing – review & editing. **Jessie S. Jeon:** Funding acquisition, Project administration, Resources, Supervision, Writing – original draft, Writing – review & editing.

Declaration of competing interest

None.

Acknowledgement

This work was supported by the National Research Foundation of Korea (NRF) grant funded by the Ministry of Science and ICT (MSIT) of Korea (No. 2021R1A2B5B03001416, No. 2020R1A2C1100471, No. 2020R1A5A8018367) and the BK21 FOUR Program of the NRF grant funded by the Ministry of Education (MOE) of Korea.

Appendix A. Supplementary data

Supplementary data to this article can be found online at https://doi.org/10.1016/j.bioactmat.2023.12.021.

References

[1] T.A. Martin, L. Ye, A.J. Sanders, J. Lane, W.G. Jiang, Madame Curie Bioscience Database [Internet], Landes Bioscience, 2013.
[2] T.N. Seyfried, L.C. Huysentruyt, On the origin of cancer metastasis, Crit. Rev. Oncog. 18 (2013) 43–73.
[3] R.L. Anderson, et al., A framework for the development of effective anti-metastatic agents, Nat. Rev. Clin. Oncol. 16 (2019) 185–204.
[4] Z. Eslami-S, L.E. Cortes-Hernandez, C. Alix-Panabieres, The metastatic cascade as the basis for liquid biopsy development, Front. Oncol. 10 (2020).
[5] A.D. Rhim, et al., EMT and dissemination precede pancreatic tumor formation, Cell 148 (2012) 349–361.
[6] Z. Deng, S. Wu, Y. Wang, D. Shi, Circulating tumor cell isolation for cancer diagnosis and prognosis, EBioMedicine 83 (2022) 104237.
[7] Y. Gao, et al., Metastasis organotropism: redefining the congenial soil, Dev. Cell 49 (2019) 375–391.
[8] Y. Kim, et al., Quantification of cancer cell extravasation *in vivo*, Nat. Protoc. 11 (2016) 937–948.
[9] S. Bersini, et al., A combined microfluidic-transcriptomic approach to characterize the extravasation potential of cancer cells, Oncotarget 9 (2018) 36110–36125.
[10] A. Sontheimer-Phelps, B.A. Hassell, D.E. Ingber, Modelling cancer in microfluidic human organs-on-chips, Nat. Rev. Cancer 19 (2019) 65–81.
[11] S. Iwai, et al., Three-dimensional cultured tissue constructs that imitate human living tissue organization for analysis of tumor cell invasion, J. Biomed. Mater. Res. 107 (2019) 292–300.
[12] B.Y. Zhang, A. Korolj, B.F.L. Lai, M. Radisic, Advances in organ-on-a-chip engineering, Nat. Rev. Mater. 3 (2018) 257–278.
[13] S. Bersini, et al., A microfluidic 3D *in vitro* model for specificity of breast cancer metastasis to bone, Biomaterials 35 (2014) 2454–2461.
[14] J.M. Ayuso, M. Virumbrales-Munoz, J.M. Lang, D.J. Beebe, A role for microfluidic systems in precision medicine, Nat. Commun. 13 (2022) 3086.
[15] X. Liu, et al., Tumor-on-a-chip: from bioinspired design to biomedical application, Microsyst. Nanoeng. 7 (2021) 50.
[16] S. Kim, Z. Wan, J.S. Jeon, R.D. Kamm, Microfluidic vascular models of tumor cell extravasation, Front. Oncol. 12 (2022) 1052192.
[17] C. Hajal, et al., The CCL2-CCR2 astrocyte-cancer cell axis in tumor extravasation at the brain, Sci. Adv. 7 (2021) eabg8139.
[18] W. Liu, et al., AKR1B10 (Aldo-keto reductase family 1 B10) promotes brain metastasis of lung cancer cells in a multi-organ microfluidic chip model, Acta Biomater. 91 (2019) 195–208.
[19] T.J. Kwak, E. Lee, Rapid multilayer microfabrication for modeling organotropic metastasis in breast cancer, Biofabrication 13 (2020) 015002.
[20] M.R. Hamblin, Shining light on the head: photobiomodulation for brain disorders, BBA Clin. 6 (2016) 113–124.
[21] G.S. Offeddu, et al., The cancer glycocalyx mediates intravascular adhesion and extravasation during metastatic dissemination, Commun. Biol. 4 (2021) 255.
[22] M.B. Chen, et al., Inflamed neutrophils sequestered at entrapped tumor cells via chemotactic confinement promote tumor cell extravasation, Proc. Natl. Acad. Sci. USA 115 (2018) 7022–7027.
[23] M. Crippa, et al., A microphysiological early metastatic niche on a chip reveals how heterotypic cell interactions and inhibition of integrin subunit β 3 impact breast cancer cell extravasation, Lab Chip 21 (2021) 1061–1072.

[24] S. Azadi, E. Mohammadi, M. Tafazzoli-Shadpour, M. Tabatabaei, Effects of chemically EGFR targeting on non-targeted physical cell behaviors in 2D and 3D microfluidic cultures of invasive and non-invasive breast cancer cell lines, Biochem. Biophys. Res. Commun. 622 (2022) 1–7.
[25] F.R. Balkwill, M. Capasso, T. Hagemann, J. Cell Sci. 125 (2012) 23.
[26] W. Huang, et al., New insights into the tumor microenvironment utilizing protein array technology, Int. J. Mol. Sci. 19 (2018) 559.
[27] M. Wang, et al., Role of tumor microenvironment in tumorigenesis, J. Cancer 8 (2017) 761–773.
[28] J.I. Luna, S.K. Grossenbacher, W.J. Murphy, R.J. Canter, Targeting cancer stem cells with natural killer cell immunotherapy, Expet Opin. Biol. Ther. 17 (2017) 313–324.
[29] J.A. Hickman, et al., Three-dimensional models of cancer for pharmacology and cancer cell biology: capturing tumor complexity *in vitro/ex vivo*, Biotechnol. J. 9 (2014) 1115–1128.
[30] B.M. Baker, C.S. Chen, Deconstructing the third dimension–how 3D culture microenvironments alter cellular cues, J. Cell Sci. 125 (2012) 3015–3024.
[31] M. Choi, et al., Polymer thin film-induced tumor spheroids acquire cancer stem cell-like properties, Cancer Res. 78 (2018) 6890–6902.
[32] M. Lee, et al., Surface hydrophobicity modulates the key characteristics of cancer spheroids through the interaction with the adsorbed proteins, Adv. Funct. Mater. 31 (2021) 2100775.
[33] Y. Javanmardi, et al., Endothelium and subendothelial matrix mechanics modulate cancer cell transendothelial migration, Adv. Sci. (2023) 2206554.
[34] F. Kai, A.P. Drain, V.M. Weaver, The extracellular matrix modulates the metastatic journey, Dev. Cell 49 (2019) 332–346.
[35] D.S. Micalizzi, S. Maheswaran, D.A. Haber, A conduit to metastasis: circulating tumor cell biology, Genes Dev. 31 (2017) 1827–1840.
[36] A.S. Azevedo, G. Follain, S. Patthabhiraman, S. Harlepp, J.G. Goetz, Metastasis of circulating tumor cells: favorable soil or suitable biomechanics, or both? Cell Adhes. Migrat. 9 (2015) 345–356.
[37] W. Tinganelli, M. Durante, Tumor hypoxia and circulating tumor cells, Int. J. Mol. Sci. 21 (2020) 9592.
[38] B. Strilic, S. Offermanns, Intravascular survival and extravasation of tumor cells, Cancer Cell 32 (2017) 282–293.
[39] N. Osmani, et al., Metastatic tumor cells exploit their adhesion repertoire to counteract shear forces during intravascular arrest, Cell Rep. 28 (2019) 2491.
[40] N. Reymond, B.B. d'Agua, A.J. Ridley, Crossing the endothelial barrier during metastasis, Nat. Rev. Cancer 13 (2013) 858–870.
[41] G. Bergers, S.M. Fendt, The metabolism of cancer cells during metastasis, Nat. Rev. Cancer 21 (2021) 162–180.
[42] Q. Wei, Y. Qian, J. Yu, C.C. Wong, Metabolic rewiring in the promotion of cancer metastasis: mechanisms and therapeutic implications, Oncogene 39 (2020) 6139–6156.
[43] B. Aslam, M. Basit, M.A. Nisar, M. Khurshid, M.H. Rasool, Proteomics: technologies and their applications, J. Chromatogr. Sci. (2016) 1–15.
[44] X. Yue, J.K. Lukowski, E.M. Weaver, S.B. Skube, A.B. Hummon, Quantitative proteomic and phosphoproteomic comparison of 2D and 3D colon cancer cell culture models, J. Proteome Res. 15 (2016) 4265–4276.
[45] Z. Wei, X. Liu, C. Cheng, W. Yu, P. Yi, Metabolism of amino acids in cancer, Front. Cell Dev. Biol. 8 (2020) 603837.
[46] M.T. Snaebjornsson, S. Janaki-Raman, A. Schulze, Greasing the wheels of the cancer machine: the role of lipid metabolism in cancer, Cell Metabol. 31 (2020) 62–76.
[47] M. Jang, S.S. Kim, J. Lee, Cancer cell metabolism: implications for therapeutic targets, Exp. Mol. Med. 45 (2013) e45.
[48] N. Koundouros, G. Poulogiannis, Reprogramming of fatty acid metabolism in cancer, Br. J. Cancer 122 (2020) 4–22.
[49] O. Warburg, On the origin of cancer cells, Science 123 (1956) 309–314.
[50] Y. Wu, et al., Targeting oxidative phosphorylation as an approach for the treatment of ovarian cancer, Front. Oncol. 12 (2022).
[51] J. Greene, A. Segaran, S. Lord, Seminars in Cancer Biology, Elsevier, 2022.
[52] C. Cencioni, V. Comunanza, E. Middonti, E. Vallariello, F. Bussolino, The role of redox system in metastasis formation, Angiogenesis 24 (2021) 435–450.
[53] V. Raimondi, F. Ciccarese, V. Ciminale, Oncogenic pathways and the electron transport chain: a dangeROS liaison, Br. J. Cancer 122 (2020) 168–181.
[54] K.G. de la Cruz López, M.E. Toledo Guzmán, E.O. Sánchez, A. García Carrancá, mTORC1 as a regulator of mitochondrial functions and a therapeutic target in cancer, Front. Oncol. 9 (2019) 1373.
[55] G.J. van der Vusse, Albumin as fatty acid transporter, Drug Metabol. Pharmacokinet. 24 (2009) 300–307.
[56] B.T. Finicle, V. Jayashankar, A.L. Edinger, Nutrient scavenging in cancer, Nat. Rev. Cancer 18 (2018) 619–633.
[57] R. Garcia, R.A. Franklin, J.A. McCubrey, EGF induces cell motility and multi-drug resistance gene expression in breast cancer cells, Cell Cycle 5 (2006) 2820–2826.
[58] T. Liu, et al., Cancer-associated fibroblasts: an emerging target of anti-cancer immunotherapy, J. Hematol. Oncol. 12 (2019) 86.
[59] S. Li, et al., MCP-1-induced ERK/GSK-3beta/Snail signaling facilitates the epithelial-mesenchymal transition and promotes the migration of MCF-7 human breast carcinoma cells, Cell. Mol. Immunol. 14 (2017) 621–630.
[60] R. Han, et al., Estrogen promotes progression of hormone-dependent breast cancer through CCL2-CCR2 axis by upregulation of Twist via PI3K/AKT/NF-κB signaling, Sci. Rep. 8 (2018) 1–13.
[61] K.M. Nieman, et al., Adipocytes promote ovarian cancer metastasis and provide energy for rapid tumor growth, Nat. Med. 17 (2011) 1498–1503.
[62] H. Yasui, et al., CCL2 secreted from cancer-associated mesothelial cells promotes peritoneal metastasis of ovarian cancer cells through the P38-MAPK pathway, Clin. Exp. Metastasis 37 (2020) 145–158.
[63] R.D. Loberg, et al., CCL2 is a potent regulator of prostate cancer cell migration and proliferation, Neoplasia 8 (2006) 578–586.
[64] S.-Y. Huang, S.-F. Chang, K.-F. Liao, S.-C. Chiu, Tanshinone IIA inhibits epithelial-mesenchymal transition in bladder cancer cells via modulation of STAT3-CCL2 signaling, Int. J. Mol. Sci. 18 (2017) 1616.
[65] T.M. Pausch, et al., Metastasis-associated fibroblasts promote angiogenesis in metastasized pancreatic cancer via the CXCL8 and the CCL2 axes, Sci. Rep. 10 (2020) 5420.
[66] A. Kosowska, et al., Exenatide modulates tumor–endothelial cell interactions in human ovarian cancer cells, Endocr. Connections 6 (2017) 856.
[67] L. Al-Alem, T.E. Curry Jr., Ovarian cancer: involvement of the matrix metalloproteinases, Reproduction (Cambridge, England) 150 (2015) R55.
[68] S. Fili, M. Karalaki, B. Schaller, Mechanism of bone metastasis: the role of osteoprotegerin and of the host-tissue microenvironment-related survival factors, Cancer Lett. 283 (2009) 10–19.
[69] G.R. Mundy, Metastasis to bone: causes, consequences and therapeutic opportunities, Nat. Rev. Cancer 2 (2002) 584–593.
[70] G. Choi, et al., Polymer-coated surface as an enzyme-free culture platform to improve human mesenchymal stem cell (hMSC) characteristics in extended passaging, ACS Appl. Bio Mater. 3 (2020) 7654–7665.